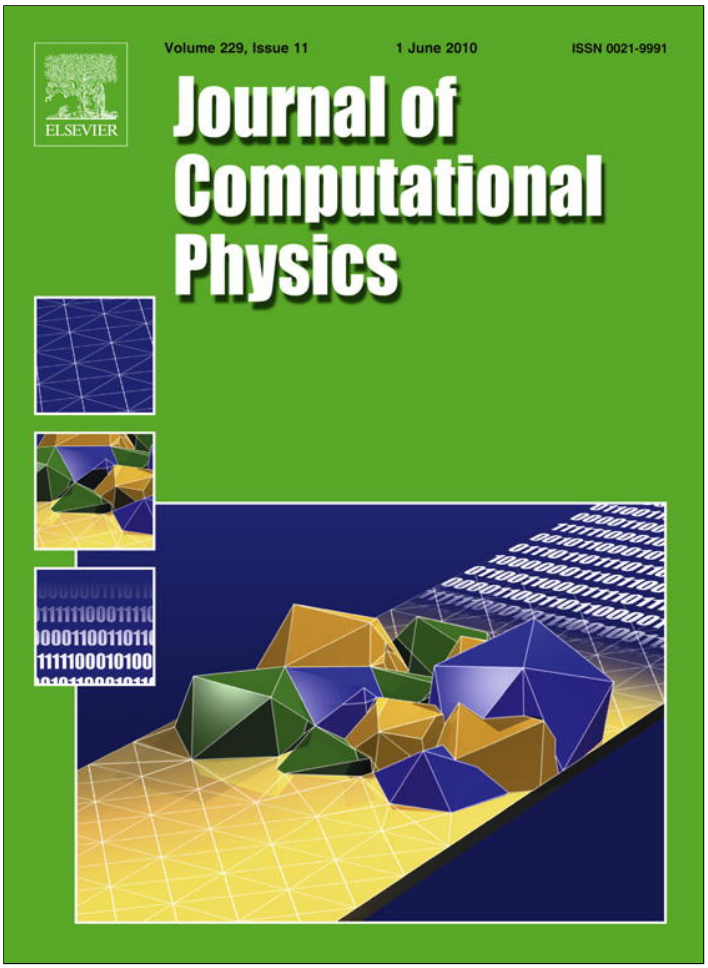

Journal of Computational Physics 229 (2010) 4315–4326

Contents lists available at ScienceDirect

Journal of Computational Physics

journal homepage: www.elsevier.com/locate/jcp

A fast iterative model for discrete velocity calculations on triangular grids

Lajos Szalmás, Dimitris Valougeorgis *

Department of Mechanical Engineering, University of Thessaly, Pedion Areos, Volos 38334, Greece

ARTICLE INFO

Article history:
Received 26 July 2009
Accepted 15 February 2010
Available online 21 February 2010

Keywords:
Discrete velocity method
Discrete kinetic equations
Acceleration
Stability analysis
Rarefied gas flows

ABSTRACT

A fast synthetic type iterative model is proposed to speed up the slow convergence of discrete velocity algorithms for solving linear kinetic equations on triangular lattices. The efficiency of the scheme is verified both theoretically by a discrete Fourier stability analysis and computationally by solving a rarefied gas flow problem. The stability analysis of the discrete kinetic equations yields the spectral radius of the typical and the proposed iterative algorithms and reveal the drastically improved performance of the latter one for any grid resolution. This is the first time that stability analysis of the full discrete kinetic equations related to rarefied gas theory is formulated, providing the detailed dependency of the iteration scheme on the discretization parameters in the phase space. The corresponding characteristics of the model deduced by solving numerically the rarefied gas flow through a duct with triangular cross section are in complete agreement with the theoretical findings. The proposed approach may open a way for fast computation of rarefied gas flows on complex geometries in the whole range of gas rarefaction including the hydrodynamic regime.

1. Introduction

Fully deterministic discrete velocity (or ordinates) algorithms have been extensively used in the direct numerical solution of the Boltzmann equation or alternatively of kinetic model equations [1–4]. Of course, the involved computational effort is significant since solving for the unknown distribution function, in a general-geometry problem, would require a six-dimensional phase space grid (three variables in the physical space and three variables in the molecular velocity space), which imposes severe demands on computer resources (time and memory). In spite of this, the discrete velocity (DV) method is considered as an efficient approach for solving problems in rarefied gas dynamics [5]. Even more, in certain physical systems where, due to the flow conditions and parameters, linearization of the governing kinetic equations and reduction of the number of spatial and velocity coordinates are permitted, the DV method has shown to be probably the most powerful computational scheme for providing reliable results in the whole range of the Knudsen number [6,7]. Such problems commonly appear in several technological fields including the emerging field of nano and microfluidics [8].

The direct differencing of kinetic equations implementing the discrete velocity approach yields a discretized coupled integro–differential system, which is solved in an iterative manner. The convergence speed of this iterative algorithm is satisfactory in highly rarefied atmospheres (large Knudsen numbers) but it slows down significantly as the atmosphere becomes less rarefied and finally, it becomes very slow at intermediate and small Knudsen numbers (part of the transition as well as in the slip regimes). This slow convergence has been recently circumvented by introducing a synthetic acceleration methodology to speed up the DV convergence rate in dense atmospheres [9–11]. That is an important advancement of the DV algorithm since it upgrades its overall performance and it allows its efficient implementation in all flow regimes. The

* Corresponding author. Tel.: +30 2421074058; fax: +30 2421074085.
E-mail address: diva@mie.uth.gr (D. Valougeorgis).

0021-9991/$ - see front matter © 2010 Elsevier Inc. All rights reserved.
doi:10.1016/j.jcp.2010.02.015

discretized version of this rapidly convergent iteration scheme has been applied so far to flow configurations, which can be adequately described on standard orthogonal grids.

It is important to note that fast iterative algorithms for discrete ordinates particle calculations have been originated and then extensively developed and efficiently implemented in the field of neutron and radiative transfer [12,13]. However, corresponding work in rarefied gas dynamics is very limited.

In the present work a fast iterative algorithm is proposed for the efficient computational solution of linear kinetic equations on triangular lattices. This non-regular lattice consisting of triangular grid elements has been recently introduced [14] and it is very useful for generalizing kinetic type solutions to rarefied flows in domains with complex boundaries. The discretization of the accelerated scheme on such non-standard grids is not trivial. Also, the convergence rates of both the typical and accelerated discrete algorithms are estimated by a discrete Fourier stability analysis. As far as the authors are aware of, this is the first time that a stability analysis of discrete kinetic equations in the field of rarefied gas dynamics is presented. It is found theoretically that the accelerated method performs significantly faster than the typical one. It is also shown that the discrete models with increasing resolution rapidly reach the convergence rate of the continuous equations. The theoretical findings are verified computationally be solving, as a benchmark problem, the flow of a gas through a triangular channel, described by the linearized two-dimensional Bhatnagar–Gross–Krook (BGK) kinetic equation [14]. The dependency of the iteration scheme on the discretization parameters in the phase space is investigated. The simulation results are in agreement with the theoretical findings.

The presented work can be applied to more advanced kinetic model equations, such as the ES and the Shakhov models for single gases [15], as well as the McCormack model for gaseous mixtures [16,17], in a straightforward manner.

2. Iteration schemes of kinetic equations

A description of the typical and upgraded (acceleration) iteration schemes applied to the continuous form of the governing kinetic equations is provided. In addition, the model problem used as a benchmark to test the overall efficiency of the proposed scheme is introduced. All quantities are in dimensionless form.

2.1. Kinetic iteration

We base our discussion on the two-dimensional linearized BGK model equation

$$\boldsymbol{c}\cdot\nabla f^{(t+1/2)}(c,\theta,\boldsymbol{x})+\delta f^{(t+1/2)}(c,\theta,\boldsymbol{x})=\delta F_{0,0}^{(t)}(\boldsymbol{x})+S(\boldsymbol{x}), \tag{1}$$

with

$$F_{0,0}^{(t+1)}(\boldsymbol{x})=\frac{1}{\pi}\int_0^{2\pi}\int_0^{\infty} f^{(t+1/2)}(c,\theta,\boldsymbol{x})\exp(-c^2)c\,dc\,d\theta, \tag{2}$$

which describes the fully developed flow of a gas through a channel of arbitrary cross section [14,18]. In Eqs. (1) and (2), $f^{(t+1/2)}(c,\theta,\boldsymbol{x})$ is the unknown distribution function, $\boldsymbol{x}=(x_1,x_2)$ is the position vector, $\boldsymbol{c}\leftrightarrow(c,\theta)$ is the molecular velocity vector with c and θ denoting the magnitude and the polar angle respectively, $S(\boldsymbol{x})$ is an optional source term, $F_{0,0}^{(t)}(\boldsymbol{x})$ is the bulk velocity and t is the iteration index. It is noted that the bulk velocity corresponds to the zeroth-order Hermitian moment of the distribution function. Finally, δ, known as the rarefaction parameter, is a very important dimensionless flow quantity, which characterizes the rarefaction degree of the physical system. The rarefaction parameter is proportional to the inverse Knudsen number. Roughly speaking, the flow is in the free molecular regime for $\delta<0.1$, in the transition regime for $0.1\leqslant\delta\leqslant 10$ and in the hydrodynamic regime for $\delta>10$.

Along the boundary of the flow domain, the Maxwell diffuse reflection model is implemented. Then, the distribution function representing particles departing from the wall is written by

$$f(\boldsymbol{c},\hat{\boldsymbol{x}})=0,\quad \text{for } \boldsymbol{c}\cdot\boldsymbol{n}>0, \tag{3}$$

where $\hat{\boldsymbol{x}}$ denotes the boundary position vector and $\boldsymbol{n}$ is the unit normal vector pointing towards the interior of the flow domain. A quantity of practical interest, used later on, is the dimensionless flow rate

$$G=\frac{2}{A}\int\int_A F_{0,0}(\boldsymbol{x})dx_1dx_2. \tag{4}$$

Here, A is the area of the cross section. It is assumed that the hydrodynamic diameter of the channel $D_h=4A/\Gamma$ is unity, where Γ denotes the perimeter of the channel.

The integro–differential system defined by Eqs. (1) and (2) is solved in an iterative manner as indicated by the iteration index t. In particular at the beginning of each iteration, one introduces an old estimate $F_{0,0}^{(t)}$ in the right hand side of Eq. (1). Using this estimate Eq. (1) is solved to obtain an estimate for $f^{(t+1/2)}$, which is introduced into Eq. (2) to obtain the new estimate $F_{0,0}^{(t+1)}$. This iteration process, which is named "kinetic iteration" is repeated until the difference between successive estimates of $F_{0,0}^{(t)}$ is less than a pre-assigned convergence criterion ϵ. It has been shown that the above described iteration process

converges fast for small values of δ and unacceptably slow for large values of δ [9,10,17]. This situation is remedied by the fast iteration scheme introduced in the following subsection.

2.2. Synthetic iteration

The rapidly convergent iteration scheme involves an additional step in each iteration. In particular, following the calculated value of $f^{(t+1/2)}(c,\theta,\boldsymbol{x})$ from Eq. (1), the updated velocity $F_{0,0}^{(t+1)}$, instead of applying Eq. (2), is obtained by solving the diffusion equation

$$\Delta F_{0,0}^{(t+1)}(\boldsymbol{x}) = -\frac{1}{2}\partial_{x_1}^2 F_{2,0}^{(t+1/2)}(\boldsymbol{x}) - \frac{1}{2}\partial_{x_2}^2 F_{0,2}^{(t+1/2)}(\boldsymbol{x}) - \partial_{x_1}\partial_{x_2} F_{1,1}^{(t+1/2)}(\boldsymbol{x}) - \delta S(\boldsymbol{x}), \tag{5}$$

where $\Delta = \partial_{x_1}^2 + \partial_{x_2}^2$. This equation is derived by taking the zeroth-and first-order moments of Eq. (1) and manipulating accordingly the resulting moment equations [9,11]. Also, at the right hand side of Eq. (5) the higher-order moments $F_{2,0}, F_{0,2}$ and $F_{1,1}$ are defined by

$$F_{m,n}^{(t+1/2)}(\boldsymbol{x}) = \frac{1}{\pi}\int_0^{2\pi}\int_0^{\infty} f^{(t+1/2)}(c,\theta,\boldsymbol{x}) H_{m,n}(\boldsymbol{c}) \exp(-c^2) c\,dc\,d\theta, \tag{6}$$

with $m,n = 0,1,2$ and $m+n = 2$. In Eq. (6), $H_{m,n}(\boldsymbol{c}) = H_m(c\cos\theta)H_n(c\sin\theta)$ stands for the two-dimensional Hermite polynomial with $H_m(\mu)$ and $H_n(\eta)$ being the mth and nth Hermite polynomial in one dimension, respectively.

The iteration process, which now is consisting of two stages, is defined as follows. At the beginning of an iteration, one has the value of $F_{0,0}^{(t)}$, known from the previous iteration. In the first stage of the iteration, Eq. (1), is solved to yield $f^{(t+1/2)}(c,\theta,\boldsymbol{x})$ and then the higher-order moments are calculated from Eq. (6). In the second stage of an iteration, Eq. (5) is solved for the updated velocity $F_{0,0}^{(t+1)}$. The iteration process, which is named "synthetic iteration" is terminated when the convergence criterion imposed on $F_{0,0}^{(t)}$ is fulfilled. It is obvious that a synthetic compared to a kinetic iteration is more costly. However, as it is shown later, the number of required iterations in the synthetic scheme is significantly reduced and therefore, the overall efficiency of the scheme is increased.

It is noted that the synthetic iteration procedure defined by Eq. (5) is used in the interior nodes of the flow domain. Therefore, the zeroth-order moment is not accelerated at the boundaries and its estimate is based on the values of the distribution function at the boundaries obtained at the first stage of the iteration. This treatment does not cause any significant deviation in the overall performance of the synthetic scheme when the discretized model is considered since the number of boundary nodes is negligible compared to the interior ones.

3. Discretization

The discretziation procedure of the kinetic and synthetic equations solved on a triangular grid is presented. Both spatial and molecular velocity spaces are discretized. The discretized spatial and velocity coordinates are denoted by $\boldsymbol{x}_p$ and (c_q,θ_r) respectively, with $1 \leqslant p \leqslant L, 1 \leqslant q \leqslant M$ and $1 \leqslant r \leqslant N$. Here, L is the total number of spatial grid points and $M \times N$ is the number of the discrete velocity vectors, with M and N denoting the magnitudes and the polar angles respectively used in the discretization.

Fig. 1, presents one computational cell of the triangular grid, consisting of the central node A, with spatial coordinate $\boldsymbol{x}_p$ and six surrounding nodes connected to the central one via the spatial vectors $\boldsymbol{r}_j, j = 1,\ldots,6$. The spatial coordinates of the six

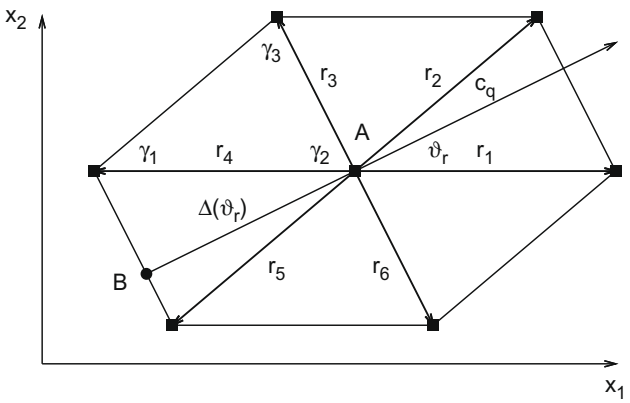

Fig. 1. Geometry of triangular grid. The central node A is surrounded by six neighboring nodes, while B indicates the upwind point for the velocity angle θ_r. The angles of all triangles are denoted by $\gamma_k, k = 1,2,3$.

surrounding nodes are $\boldsymbol{x}_p + \boldsymbol{r}_j$. Also, a typical velocity vector with magnitude $0 < c_q < \infty$ and polar angle $0 \leqslant \theta_r < 2\pi$, passing through the central node A, is shown.

3.1. Discrete kinetic iteration

The discretized form of Eq. (1) reads

$$\frac{c_q}{\Delta(\theta_r)}\left[f^{(t+1/2)}(c_q,\theta_r,\boldsymbol{x}_p)-\sum_{j=1}^{6}a_j(\theta_r)f^{(t+1/2)}(c_q,\theta_r,\boldsymbol{x}_p+\boldsymbol{r}_j)\right]+\delta f^{(t+1/2)}(c_q,\theta_r,\boldsymbol{x}_p)=\delta F_{0,0}^{(t)}(\boldsymbol{x}_p)+S(\boldsymbol{x}_p). \tag{7}$$

In this equation, the first term in the bracket on the left hand side is the upwind finite-difference approximation of the streaming term in Eq. (1). Specifically, $\Delta(\theta_r)$ is the spacing between the central node A and the upwind point B shown in Fig. 1, while $a_j(\theta_r)$ are weight functions related to the linear interpolation used to get the distribution function at the upwind point B in terms of the distribution functions at the two adjacent nodes. For each angle $0 \leqslant \theta_r < 2\pi$, with $1 \leqslant r \leqslant N$, there are only two non-zero $a_i(\theta_r)$ weights from the six-element set. The explicit expressions of $a_j(\theta_r)$ and $\Delta(\theta_r)$ are presented in Appendix A.

In the discretized formulation, the updated value of the macroscopic velocity is obtained from Eq. (2) such that

$$F_{0,0}^{(t+1)}(\boldsymbol{x}_p)=\frac{2}{N}\sum_{q=1}^{M}\sum_{r=1}^{N}w_q f^{(t+1/2)}(c_q,\theta_r,\boldsymbol{x}_p)c_q. \tag{8}$$

In Eq. (8), the integration over the velocity polar angle and magnitude is performed based on the trapezoidal rule and the Gauss–Legendre quadrature with w_q denoting the quadrature weights, respectively.

3.2. Discrete synthetic iteration

Next, we turn our attention to the synthetic accelerated equation. The discrete form of Eq. (5) is given by

$$\begin{aligned}\sum_{j=1}^{6}\left[b_{1,j}+b_{2,j}\right]\left[F_{0,0}^{(t+1)}(\boldsymbol{x}_p+\boldsymbol{r}_j)-F_{0,0}^{(t+1)}(\boldsymbol{x}_p)\right]&=-\frac{1}{2}\sum_{j=1}^{6}b_{1,j}\left[F_{2,0}^{(t+1/2)}(\boldsymbol{x}_p+\boldsymbol{r}_j)-F_{2,0}^{(t+1/2)}(\boldsymbol{x}_p)\right]\\&\quad-\frac{1}{2}\sum_{j=1}^{6}b_{2,j}\left[F_{0,2}^{(t+1/2)}(\boldsymbol{x}_p+\boldsymbol{r}_j)-F_{0,2}^{(t+1/2)}(\boldsymbol{x}_p)\right]\\&\quad-\sum_{j=1}^{6}b_{3,j}\left[F_{1,1}^{(t+1/2)}(\boldsymbol{x}_p+\boldsymbol{r}_j)-F_{1,1}^{(t+1/2)}(\boldsymbol{x}_p)\right]-\delta S(\boldsymbol{x}_p).\end{aligned} \tag{9}$$

This equation is obtained by using the finite-difference approximation of the spatial derivatives in Eq. (5). The finite-difference method is based on the values of the macroscopic quantities at the central and six surrounding nodes. In this description, $b_{p,j}$ are weight functions relevant to the second-order spatial derivatives. These weights are obtained by the Taylor expansion of the spatially dependent quantities around the central node. The explicit expressions of the weights, $b_{p,j}$, and the details of the derivation are presented in the Appendix B. The linear algebraic system defined by Eq. (9) is solved using a successive over-relaxation solver.

Finally, the integral expression of the Hermite moments in Eq. (6) is replaced by the summation

$$F_{m,n}^{(t+1/2)}(\boldsymbol{x}_p)=\frac{2}{N}\sum_{q=1}^{M}\sum_{r=1}^{N}w_q f^{(t+1/2)}(c_q,\theta_r,\boldsymbol{x}_p)H_{m,n}(c_q,\theta_r)c_q. \tag{10}$$

It is noted that Eq. (10) is valid for the higher-order moments $F_{2,0}^{(t+1)}, F_{0,2}^{(t+1)}$ and $F_{1,1}^{(t+1)}$, while the zeroth-order, i.e., the velocity $F_{0,0}^{(t+1)}$, is obtained solving Eq. (9).

4. Discrete stability analysis

In this section, the convergence rate of both the discrete kinetic and synthetic iteration schemes is studied by applying a Fourier stability analysis. This analysis is used to estimate theoretically the spectral radius of the iterative methods, as well as their dependency on the discretization parameters. Now, the functions $f^{(t)}(c_q,\theta_r,\boldsymbol{x}_p)$ and $F_{m,n}^{(t)}(\boldsymbol{x}_p)$ are considered as perturbations between successive iterates satisfying the discrete equations formulated in Section 3, with $S(\boldsymbol{x}_p) = 0$.

To begin with, we follow [9,12,13] and consider the single Fourier mode ansatz

$$f^{(t+1/2)}(c_q,\theta_r,\boldsymbol{x}_p)=\omega(\boldsymbol{k})^t f_F(c_q,\theta_r,\boldsymbol{k})\exp(i\boldsymbol{k}\boldsymbol{x}_p) \tag{11}$$

and

$$F_{0,0}^{(t)}(\boldsymbol{x}_p)=\omega(\boldsymbol{k})^t\exp(i\boldsymbol{k}\boldsymbol{x}_p), \tag{12}$$

where $f_F(c_q,\theta_r,\boldsymbol{k})$ is the Fourier amplitude and $\omega(\boldsymbol{k})$ is the iteration eigenvalue corresponding to the wave number $\boldsymbol{k}$, while

$$F_{0,0}^{(t+1)}(\boldsymbol{x}_p) = \omega(\boldsymbol{k})F_{0,0}^{(t)}(\boldsymbol{x}_p) = \omega(\boldsymbol{k})^{t+1}\exp(i\boldsymbol{k}\boldsymbol{x}_p). \tag{13}$$

Our objective in this section is to derive closed form expressions for the eigenvalues $\omega(\boldsymbol{k})$ for the kinetic and the synthetic iteration methods. The eigenvalues $\omega(\boldsymbol{k})$ describe the convergence behavior of the iteration method. Then, the spectral radius of the two iterations maps may be estimated by finding the upper bound for $\omega(\boldsymbol{k})$ according to

$$\sigma = \sup|\omega(\boldsymbol{k})| \tag{14}$$

and consequently the convergence rates of the kinetic and synthetic iteration schemes are determined.

4.1. Eigenvalues of kinetic iteration

First, the eigenvalues of the kinetic iteration method defined by Eqs. (7) and (8) are examined. By substituting Eqs. (11) and (12) into the discrete kinetic equation Eq. (7), with $S = 0$, we obtain the Fourier mode eigenvector

$$f_F(c_q,\theta_r,\boldsymbol{k}) = \left[\frac{c_q}{\delta\Delta(\theta_r)}(1 - A(\theta_r,\boldsymbol{k})) + 1\right]^{-1}. \tag{15}$$

Here, we have introduced the function

$$A(\theta_r,\boldsymbol{k}) = \sum_{j=1}^{6} a_j(\theta_r)\exp(i\boldsymbol{k}\boldsymbol{r}_j). \tag{16}$$

Next, substituting Eq. (11), with f_F given by Eqs. (15) and (13) into Eq. (8), yields

$$\omega_K(\boldsymbol{k}) = \frac{2}{N}\sum_{r=1}^{N}\sum_{q=1}^{M} w_q\left[\frac{c_q}{\delta\Delta(\theta_r)}(1 - A(\theta_r,\boldsymbol{k})) + 1\right]^{-1} c_q. \tag{17}$$

Here, the K index denotes the eigenvalues for the kinetic iteration scheme.

4.2. Eigenvalues of synthetic iteration

Secondly, the eigenvalues of the synthetic iteration method defined by Eqs. (7), (9) and (10) are estimated. It is easily seen that the Fourier mode eigenvector f_F given by Eq. (15) remains the same as before. Substituting Eq. (11) into Eq. (10), which provides the higher non-accelerated Hermitian moments, results to

$$F_{m,n}^{(t+1/2)}(\boldsymbol{x}_p) = \omega(\boldsymbol{k})^t\Phi_{m,n}(\boldsymbol{k})\exp(i\boldsymbol{k}\boldsymbol{x}_p), \tag{18}$$

where

$$\Phi_{m,n}(\boldsymbol{k}) = \frac{2}{N}\sum_{r=1}^{N}\sum_{q=1}^{M} w_q f_F(c_q,\theta_r,\boldsymbol{k})H_{m,n}(c_q,\theta_r)c_q, \tag{19}$$

with $m,n = 0,1,2$ and $m + n = 2$. Then, Eqs. (13) and (19) are substituted into the left and right hand side respectively of Eq. (9) to deduce after some routine manipulation the following closed form expression for the eigenvalues of the synthetic iteration scheme

$$\omega_S(\boldsymbol{k}) = -\frac{1}{2}[B_1(\boldsymbol{k})\Phi_{2,0}(\boldsymbol{k}) + B_2(\boldsymbol{k})\Phi_{0,2}(\boldsymbol{k}) + 2B_3(\boldsymbol{k})\Phi_{1,1}(\boldsymbol{k})] \times [B_1(\boldsymbol{k}) + B_2(\boldsymbol{k})]^{-1}. \tag{20}$$

Here, we have introduced the function

$$B_p(\boldsymbol{k}) = \sum_{j=1}^{6} b_{p,j}[\exp(i\boldsymbol{k}\boldsymbol{r}_j) - 1], \tag{21}$$

with $p = 1,2,3$, while the S index denotes the eigenvalues for the synthetic iteration method.

4.3. Properties of eigenvalues

Having established closed form expressions for $\omega_K(\boldsymbol{k})$ and $\omega_S(\boldsymbol{k})$, in this subsection some properties of these iteration eigenvalues are derived.

It may be shown that the eigenvalues of the discrete iteration schemes are always real. In the kinetic iteration case, the eigenvalue is obtained by Eq. (17). In regard to the complex nature of the eigenvalue, the main quantity is

$$\xi(\theta_r, \boldsymbol{k}) = \frac{1 - A(\theta_r, \boldsymbol{k})}{\Delta(\theta_r)}. \tag{22}$$

It follows from the properties $a_i(\theta_r) = a_{i+3}(\theta_r - \pi)$ and $\boldsymbol{r}_i = -\boldsymbol{r}_{i+3}$ for $i = 1,2,3$ that

$$Re[A(\theta_r, \boldsymbol{k})] = Re[A(\theta_r + \pi, \boldsymbol{k})], \tag{23}$$
$$Im[A(\theta_r, \boldsymbol{k})] = -Im[A(\theta_r + \pi, \boldsymbol{k})]. \tag{24}$$

These equations together with the property $\Delta(\theta_r) = \Delta(\theta_r + \pi)$ yield

$$Re[\xi(\theta_r, \boldsymbol{k})] = Re[\xi(\theta_r + \pi, \boldsymbol{k})], \tag{25}$$
$$Im[\xi(\theta_r, \boldsymbol{k})] = -Im[\xi(\theta_r + \pi, \boldsymbol{k})]. \tag{26}$$

Next, substituting Eqs. (25) and (26) into the expression of the eigenvalue, Eq. (17), it is readily deduced that $\omega_K(\boldsymbol{k})$ is real.

In the synthetic iteration case, the eigenvalue is obtained by Eq. (20). From symmetry principles, one can obtain that

$$Im[B_p(\boldsymbol{k})] = 0, \tag{27}$$

for $p = 1,2,3$. In addition, the Hermite polynomials have the following property

$$H_{m,n}(c_q, \theta_r) = H_{m,n}(c_q, \theta_r + \pi), \tag{28}$$

for $m,n = 0,1,2$ and $m + n = 2$. Using Eqs. (27) and (28) together with Eqs. (25) and (26) in Eq. (20), straightforward calculation shows that $\omega_S(\boldsymbol{k})$ is real. It is mentioned that the eigenvalues in the continuous situation are also real. Hence, this property survives in the presented discrete method as well.

Also, the continuous limit of the eigenvalues as the resolution tends infinitely fine is presented. In order to get the continuous limit, we deduce the limiting value of $\xi(\theta_r, \boldsymbol{k})$, which causes the discrete effect in the eigenvalues. We define the resolution $h = r_1$ as the base of the triangle element. The other spatial vectors used in the discretization are of the same order as r_1, i.e., $r_j \sim O(h)$, $j = 1,\ldots,6$. In this way, $\exp(i\boldsymbol{k}\boldsymbol{r}_j)$ is expanded up to $O(h^2)$ such that

$$\exp(i\boldsymbol{k}\boldsymbol{r}_j) = 1 + i\boldsymbol{k}\boldsymbol{r}_j + O(h^2). \tag{29}$$

As a consequence, it is found that

$$A(\theta_r, \boldsymbol{k}) = 1 + \sum_{j=1}^{6} a_j(\theta_r) i\boldsymbol{k}\boldsymbol{r}_j + O(h^2). \tag{30}$$

Then, the limiting value of $\xi(\theta_r, \boldsymbol{k})$ as $h \to 0$ is

$$\lim_{h\to 0} \xi(\theta_r, \boldsymbol{k}) = \lim_{h\to 0} \frac{1 - A(\theta_r, \boldsymbol{k})}{\Delta(\theta_r)} = -\frac{\sum_{j=1}^{6} a_j(\theta_r) i\boldsymbol{k}\boldsymbol{r}_j}{\Delta(\theta_r)} = i\boldsymbol{k}\boldsymbol{e}, \tag{31}$$

where $\boldsymbol{e} = [\cos(\theta_r), \sin(\theta_r)]$ is the unit vector in the direction of $\boldsymbol{c}$. In addition, we take the limit $M,N \to \infty$. In this way, it is obtained from Eqs. (17) and (20) that in the continuum limit

$$\omega_K(\boldsymbol{k}) = \frac{1}{\sqrt{\pi}} \int_{-\infty}^{\infty} \frac{e^{-c^2}}{c^2 (k/\delta)^2 + 1} dc \tag{32}$$

and

$$\omega_S(\boldsymbol{k}) = \frac{1}{\sqrt{\pi}} \int_{-\infty}^{\infty} \frac{1 - 2c^2}{c^2 (k/\delta)^2 + 1} e^{-c^2} dc, \tag{33}$$

respectively. These are the limiting values of the eigenvalues and are identical to previous findings [9,11], based on the continuous form of the equations.

5. Results

Both theoretical and computational results on the convergence rates of the two iteration schemes are provided. The former ones are based on the prescribed discrete Fourier stability analysis, while the latter ones on the numerical solution of the model problem with both algorithms.

5.1. Discrete effects on the convergence rates

The theoretical convergence behavior of the kinetic and synthetic iteration schemes is shown in Figs. 2–4, where the eigenvalues of the two models, given by Eqs. (17) and (20), are plotted in terms of the wave number for different values

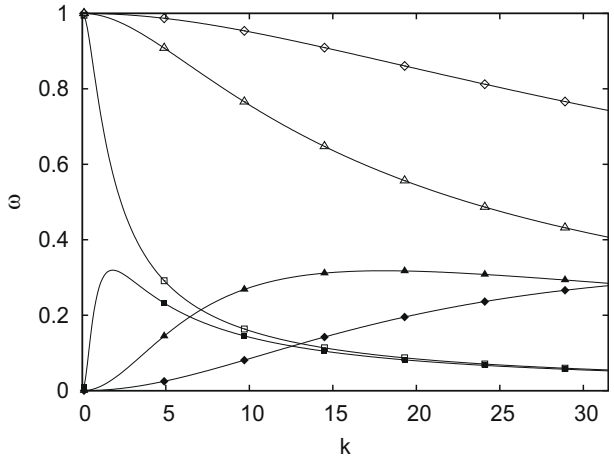

Fig. 2. Eigenvalues $\omega(\boldsymbol{k})$ versus wave number $\boldsymbol{k}$ at different values of the rarefaction parameter δ. The resolution is fixed at $h = 10^{-3}$ and $M \times N = 16 \times 144$. Symbols $\square, \triangle, \diamond$ represent kinetic results for $\delta = 1, 10$ and 30, while $\blacksquare, \blacktriangle, \blacklozenge$ represent the corresponding synthetic results.

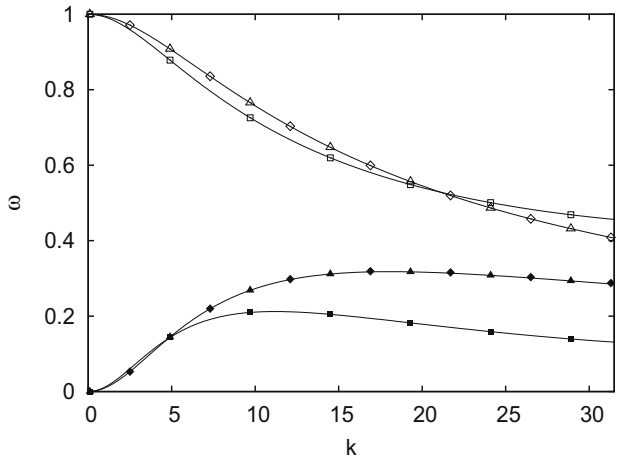

Fig. 3. Eigenvalues $\omega(\boldsymbol{k})$ versus wave number $\boldsymbol{k}$ at different values of spatial resolution h. The rarefaction parameter and the angular resolution are fixed at $\delta = 10$ and $N \times M = 16 \times 144$, respectively. Symbols $\square, \triangle, \diamond$ represent kinetic results for $h = 10^{-1}, 10^{-3}$ and $h \to 0$ (continuous limit), while $\blacksquare, \blacktriangle, \blacklozenge$ represent the corresponding synthetic results.

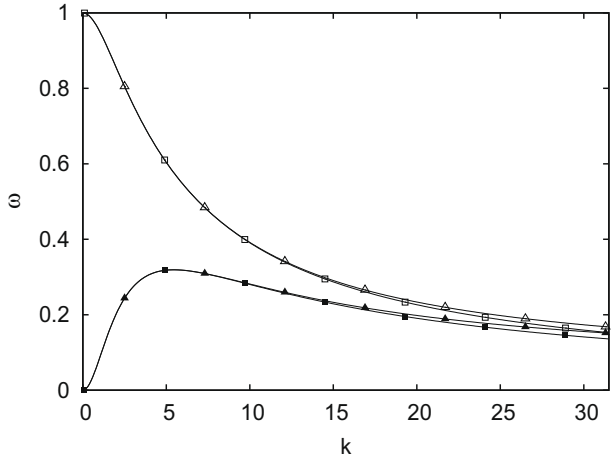

Fig. 4. Eigenvalues $\omega(\boldsymbol{k})$ versus wave number $\boldsymbol{k}$ at different values of the angular resolution $M \times N$. The rarefaction parameter and the spatial resolution are fixed at $\delta = 3$ and $h = 10^{-3}$, respectively. Symbols $\square, \triangle$ represent kinetic results for $M \times N = 16 \times 144$ and 8×24, while $\blacksquare, \blacktriangle$ represent the corresponding synthetic results.

of flow and discretization parameters. The involved parameters include the rarefaction parameter δ, which is a flow parameter, and the grid parameters h and $M \times N$ in the physical and molecular velocity spaces, respectively. In all three figures, the empty and filled symbols denote kinetic and synthetic results, respectively. Also, the wave number is pointed to the direction of x_1, with its Cartesian components given by $(k,0)$. In all cases, it is clearly seen that the kinetic iteration suppresses the error modes in the region of large wave numbers $k \gg 0$, but not the error modes in the region $k \sim 0$. On the contrary, the synthetic iteration suppresses the error modes in the whole spectrum of the wave number, therefore it is expected to converge faster.

Before we study further Figs. 2–4, it is useful at this stage to comment on the spectral radius of the two models. It is seen (Figs. 2–4) that for the kinetic iteration case, the spectral radius is always unity, i.e., $\sigma_K = 1$. This property is the main reason of the very slow convergence of the typical iterative DV scheme in part of the transition and in the slip regimes. However, by using the synthetic iteration method, the spectral radius is significantly reduced. In Table 1, the spectral radius σ_S for the synthetic iteration scheme is tabulated for different values of h and δ, while $M \times N$ is fixed at 16×144. It is seen that as h is decreased, while δ is kept constant, the spectral radius is increased. This is more evident at large values of δ. Also, as δ is increased, while h is kept constant, the spectral radius is decreased. This is more evident at large values of h.

It is noted that in the continuous limit ($h \to 0$) according to Eq. (33) $\sigma_S = 0.320$. It is clearly seen in Table 1 that the discrete spectral radii converge to the continuous result as $h \to 0$. It is also seen that as δ is increased finer resolution is required to obtain the continuous limit. This is easily explained since as δ is increased the spectral radius happens to appear at larger wave numbers or alternatively at smaller wave lengths, which require finer grid resolution. The results, shown in Table 1, for σ_S in terms of δ and h are useful for the theoretical justification of discrete synthetic simulations.

Next, studying in detail Figs. 2–4, a more comprehensive and complete description of the dependency of the convergence rates on δ, h and $M \times N$ in the whole spectrum of the wave number may be deduced. In Fig. 2, the kinetic and synthetic eigenvalues $\omega(\boldsymbol{k})$ are shown for δ equal to 1, 10 and 30, while the grid resolution is fixed at $h = 10^{-3}$ and $M \times N = 16 \times 144$. In this figure, the effect of the rarefaction parameter δ is observed. It is clear that as δ is increased (i.e., the atmosphere becomes less rarefied) the convergence rate exhibit slower attenuation as a function of the wave number. In the case of the kinetic iteration, where the spectral radius is unity, this behavior is the main reason of the slow convergence rate at large values of δ. In the case of the synthetic iteration, this behavior has no effect on the convergence rate since the discrete spectral radius is always less than 0.320.

In Fig. 3, the effect of the spatial discretization is observed. Here, results are presented for a coarse grid ($h = 10^{-1}$), for a fine grid ($h = 10^{-3}$) and for the limiting case $h \to 0$ (continuous limit), with $\delta = 10$ and $M \times N = 16 \times 144$. The convergence rates show the same qualitative behavior at the different values of spatial resolution. Also the quantitative differences between $h = 10^{-1}$ and $h = 10^{-3}$ are clearly indicated. When the resolution is sufficiently small, $\omega(\boldsymbol{k})$ obtained from the discrete model reaches the value of the continuous situation presented by Eqs. (32) and (33). It is seen that at $h = 10^{-3}$, the difference is already invisible between the two cases. This result clearly demonstrates that the discrete velocity model converges to the continuous model formulation.

In Fig. 4, the effect of the molecular velocity discretization is observed by presenting results for $M \times N = 16 \times 144$ and 8×24, with $\delta = 3$ and $h = 10^{-3}$. There is very small deviation between the corresponding curves when the velocity resolution changes. In general, as δ is decreased the dependency of the convergence rate on the velocity discretization is increased. However, it may be concluded that the presented results are typical and that the angular resolution has a little effect on the eigenvalues of the iteration map.

5.2. Computational performance

Simulations have been carried out to investigate and compare the computational performance of the two methods. The rarefied gas flow problem described in Section 2 for a channel with equilateral triangular cross section has been solved. The source term is $S(\boldsymbol{x}) = -1/2$. In all simulations, we have used $L = 500500, M = 16$ and $N = 72$ and a convergence error $\epsilon = \| G^{(t+1)} - G^{(t)} \| < 10^{-8}$.

In Table 2, the number of iterations, the computational time and the flow rate in the whole range of the rarefaction parameter are presented. The results for the kinetic and synthetic methods are indicated by the K and S labels respectively. The number of iterations are given in the 2nd and 3rd column of Table 2. It is observed that as δ is increased the number of kinetic iterations is monotonically increased, while the number of synthetic iterations is initially increased, then for

Table 1
Discrete spectral radius σ_S of synthetic scheme.

h	δ				
	0.1	1.0	5.0	10.0	50.0
10^{-1}	0.318	0.303	0.253	0.212	0.100
10^{-2}	0.319	0.318	0.311	0.303	0.253
10^{-3}	0.320	0.319	0.319	0.318	0.311
10^{-4}	0.320	0.320	0.319	0.319	0.319

Table 2
Computational performance of the kinetic (K) and synthetic (S) schemes.

δ	Iterations		CPU time (s)		$-G$		$-G_s$
	K	S	K	S	K	S	
0.0	2	2	87	90	0.9287	0.9287	
0.1	9	9	394	1246	0.8712	0.8712	
1.0	25	22	1126	3613	0.8320	0.8321	
3.0	62	33	2814	5383	0.9292	0.9305	
5.0	111	35	5007	5724	1.0560	1.0595	
7.0	171	35	7719	5728	1.1905	1.1969	
10.0	283	35	12441	5719	1.3977	1.4095	
30.0	1692	35	75773	5704	2.7996	2.8800	
50.0	4154	35	184735	5721	4.1605	4.3709	4.3556
100.0		34		4439		8.1190	8.1076
500.0		31		3901		3.8139(+1)	3.8109(+1)

$3 \leqslant \delta \leqslant 50$ remains stable and equal to the moderate number of 35 iterations and finally, at higher value of δ, the number of iterations is slightly decreased. This behavior at large δ is expected since the flow is in the hydrodynamic regime and the diffusion equation provides, by itself, a fairly good description of the flow. Analogous behavior is observed, in the 4th and 5th column of Table 2, for the CPU time. Even though the CPU time of a synthetic iteration is larger than the CPU time of a kinetic iteration, the overall CPU time of the synthetic scheme, as δ is increased is much less than the corresponding CPU time of the kinetic scheme. This is clearly due to the fact that in the synthetic algorithm the required number of iterations is drastically reduced.

Looking at the 6th and 7th columns of Table 2 it is seen that the flow rates G computed by the two algorithms are in general in good agreement. It is clear however, that the discrepancy between the results is increased as δ is increased (e.g. for $\delta = 1$ there is agreement up to 4 significant figures, while at $\delta = 10$ the agreement drops down to 3 significant figures, within ± 1 in the last digit). To clarify which algorithm provides the correct results a comparison with semi-analytical results obtained by solving the Stokes equation with first-order slip boundary conditions has been performed for $\delta = 50, 100$ and *500*. For these values of δ the slip solution is reliable [14]. It has been found that the flow rates computed by the synthetic iteration scheme are in agreement up to three significant figures with the slip results denoted by G_s and shown in the last column of Table 2. This demonstrates the very good overall computational efficiency (speed and accuracy) of the synthetic scheme in the whole range of rarefaction including the hydrodynamic regime.

Finally, the computational performance versus the relative convergence criterion ϵ is examined. In Figs. 5 and 6, the required number of iterations and the overall CPU time respectively are presented as a function of ϵ at two values of the rarefaction parameter, namely $\delta = 3$ and 50. It is observed that for $\delta = 3$ both schemes are computationally equivalent. However, for $\delta = 50$ the superiority of the synthetic scheme is clear since the number of iterations and the CPU time are reduced by one to two orders. Comparing these results with previous ones in orthogonal lattices [9], it may be concluded that the proposed discrete synthetic iterative scheme on triangular lattices performs computationally equally well.

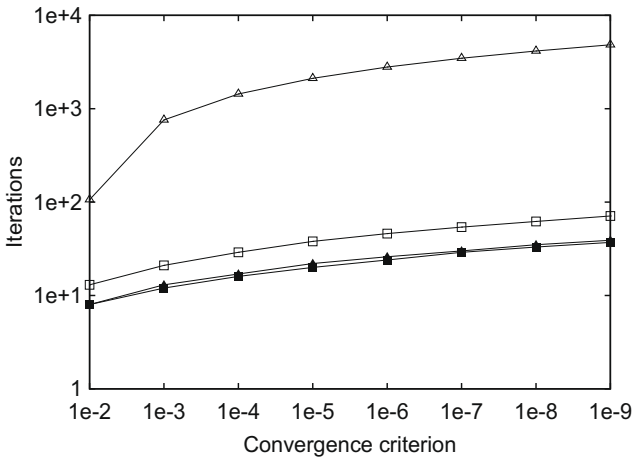

Fig. 5. Number of iterations versus convergence criterion (ϵ). Symbols □, △ represent kinetic results for $\delta = 3$ and 50, while ■, ▲ represent the corresponding synthetic results.

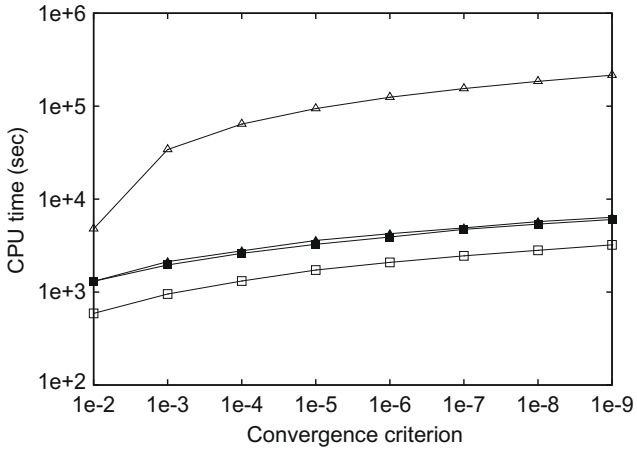

Fig. 6. CPU time in seconds versus convergence criterion (ϵ). Symbols □, △ represent kinetic results for $\delta = 3$ and 50 while ■, ▲ represent the corresponding synthetic results.

6. Concluding remarks

A fast synthetic iterative discrete velocity algorithm for solving kinetic model equations on triangular lattices has been proposed. A discrete Fourier stability analysis of the synthetic iterative and the typical kinetic schemes has been formulated and closed form expressions for the spectral radius have been derived. The effects of the rarefaction parameter characterizing the physical system and of the grid resolution both in the physical and molecular velocity spaces have been theoretically studied. It has been found that in all cases the convergence rate of the proposed synthetic algorithm is significantly faster than the corresponding one of the typical scheme. Also, the proposed model has been checked by solving the flow of a rarefied gas on a triangular grid. The simulation results are in very good agreement with the theoretical ones verifying the computational efficiency of the synthetic scheme in the whole range of gas rarefaction. The proposed model may stimulate the development of discrete kinetic models on non-standard geometries. In addition, the established discrete stability analysis can be used for other discrete models as well.

Acknowledgments

The research leading to these results has received funding from the European Community's Seventh Framework programme (FP7/2007-2013) under grant agreement No. 215504.

Appendix A. Discretization coefficients for the kinetic equation

The coefficients $a_i(\theta_r)$ and the distance $\Delta(\theta_r)$, associated to the upwind finite-difference scheme used in Eq. (7), are defined in a compact form. These quantities can be defined by using the vector $\beta_i = [\gamma_1, \gamma_1 + \gamma_3, \pi, \pi + \gamma_1, \pi + \gamma_1 + \gamma_3, 2\pi]$ and the sine theorem for the geometry given in Fig 1. It is seen that the six angle elements of β_i are the upper bounds of the six polar angle sectors of θ_r.

The coefficients $a_i(\theta_r)$ are defined to be periodic, i.e., $a_i(\theta_r) = a_i(\theta_r + 2\pi)$. In addition, they have the property $a_i(\theta_r) = a_{i+3}(\theta_r - \pi)$ for $i = 1,2,3$. Therefore, $a_i(\theta_r)$ are defined only in the $\pi \leqslant \theta_r < 2\pi$ angle interval. As it has been mentioned, there are two non-zero elements from $a_i(\theta_r)$ for each θ_r. These two adjacent weights are defined by

$$a_i(\theta_r) = \frac{\sin(\theta_r - \beta_i)}{\sin(\theta_r - \beta_{i+1})} \frac{r_{i+1}}{r_{i+2}} \tag{34}$$

and

$$a_{i+1}(\theta_r) = \frac{\sin(\theta_r - \beta_{i+2})}{\sin(\theta_r - \beta_{i+1})} \frac{r_{i+3}}{r_{i+2}}, \tag{35}$$

for $\beta_{i+2} \leqslant \theta_r < \beta_{i+3}$, where $i = 1,2,3$. These i indices recover the selected angle interval via the β_i bounds. The distance $\Delta(\theta_r)$ is also periodic, i.e., $\Delta(\theta_r) = \Delta(\theta_r + \pi)$. For the sector $\pi \leqslant \theta_r < 2\pi$ recovered with the indices $i = 4,5,6$ in β_i, it is deduced that

$$\Delta(\theta_r) = \frac{\sin(\beta_{i-1} - \beta_{i-2})}{\sin(\theta_r - \beta_{i-2})} r_i, \quad \text{for } \beta_{i-1} \leqslant \theta_r < \beta_i, \tag{36}$$

while for $0 \leqslant \theta_r < \pi$ the periodicity property can be applied.

Appendix B. Discretization coefficients for the diffusion equation

The coefficients $b_{p,j}, j = 1,\ldots,6$ for the diffuse equation Eq. (9) can be obtained via Taylor expansion. Let us consider a function $g(\boldsymbol{x})$ Taylor expanded up to second-order around the centre node denoted by $\boldsymbol{x}_p$. At the six surrounding nodes, the function is obtained by

$$g(\boldsymbol{x}_p+\boldsymbol{r}_1) = g(\boldsymbol{x}_p) + \partial_{x_1} g(\boldsymbol{x}_p) r_{1x_1} + \frac{1}{2}\partial^2_{x_1} g(\boldsymbol{x}_p) r^2_{1x_1}, \tag{37}$$

$$g(\boldsymbol{x}_p+\boldsymbol{r}_2) = g(\boldsymbol{x}_p) + \partial_{x_1} g(\boldsymbol{x}_p) r_{2x_1} + \partial_{x_2} g(\boldsymbol{x}_p) r_{2x_2} + \frac{1}{2}\partial^2_{x_1} g(\boldsymbol{x}_p) r^2_{2x_1} + \frac{1}{2}\partial^2_{x_2} g(\boldsymbol{x}_p) r^2_{2x_2} + \partial_{x_1}\partial_{x_2} g(\boldsymbol{x}_p) r_{2x_1} r_{2x_2}, \tag{38}$$

$$g(\boldsymbol{x}_p+\boldsymbol{r}_3) = g(\boldsymbol{x}_p) + \partial_{x_1} g(\boldsymbol{x}_p) r_{3x_1} + \partial_{x_2} g(\boldsymbol{x}_p) r_{3x_2} + \frac{1}{2}\partial^2_{x_1} g(\boldsymbol{x}_p) r^2_{3x_1} + \frac{1}{2}\partial^2_{x_2} g(\boldsymbol{x}_p) r^2_{3x_2} + \partial_{x_1}\partial_{x_2} g(\boldsymbol{x}_p) r_{3x_1} r_{3x_2}, \tag{39}$$

$$g(\boldsymbol{x}_p+\boldsymbol{r}_4) = g(\boldsymbol{x}_p) + \partial_{x_1} g(\boldsymbol{x}_p) r_{4x_1} + \frac{1}{2}\partial^2_{x_1} g(\boldsymbol{x}_p) r^2_{4x_1}, \tag{40}$$

$$g(\boldsymbol{x}_p+\boldsymbol{r}_5) = g(\boldsymbol{x}_p) + \partial_{x_1} g(\boldsymbol{x}_p) r_{5x_1} + \partial_{x_2} g(\boldsymbol{x}_p) r_{5x_2} + \frac{1}{2}\partial^2_{x_1} g(\boldsymbol{x}_p) r^2_{5x_1} + \frac{1}{2}\partial^2_{x_2} g(\boldsymbol{x}_p) r^2_{5x_2} + \partial_{x_1}\partial_{x_2} g(\boldsymbol{x}_p) r_{5x_1} r_{5x_2}, \tag{41}$$

$$g(\boldsymbol{x}_p+\boldsymbol{r}_6) = g(\boldsymbol{x}_p) + \partial_{x_1} g(\boldsymbol{x}_p) r_{6x_1} + \partial_{x_2} g(\boldsymbol{x}_p) r_{6x_2} + \frac{1}{2}\partial^2_{x_1} g(\boldsymbol{x}_p) r^2_{6x_1} + \frac{1}{2}\partial^2_{x_2} g(\boldsymbol{x}_p) r^2_{6x_2} + \partial_{x_1}\partial_{x_2} g(\boldsymbol{x}_p) r_{6x_1} r_{6x_2}. \tag{42}$$

Taking the appropriate linear combinations of Eqs. (37)–(42), the second-order derivatives in the synthetic equation Eq. (9) can be expressed as

$$\partial^2_{x_1} g(\boldsymbol{x}_p) = \sum_{i=1}^{6} b_{1,i}[g(\boldsymbol{x}_p+\boldsymbol{r}_i) - g(\boldsymbol{x}_p)], \tag{43}$$

$$\partial^2_{x_2} g(\boldsymbol{x}_p) = \sum_{i=1}^{6} b_{2,i}[g(\boldsymbol{x}_p+\boldsymbol{r}_i) - g(\boldsymbol{x}_p)], \tag{44}$$

$$\partial_{x_1}\partial_{x_2} g(\boldsymbol{x}_p) = \sum_{i=1}^{6} b_{3,i}[g(\boldsymbol{x}_p+\boldsymbol{r}_i) - g(\boldsymbol{x}_p)]. \tag{45}$$

The explicit expressions of $b_{p,i}$ are obtained based on Eqs. (37)–(42). The coefficients have the property $b_{p,i} = b_{p,i+3}$ for $i = 1,2,3$. The nonzero elements of $b_{p,i}$ for $i = 1,2,3$ are

$$b_{1,1} = 1/r_1^2, \tag{46}$$

$$b_{2,1} = -\cos(\gamma_1)\cos(\gamma_2)/[r_1^2\sin(\gamma_1)\sin(\gamma_2)], \tag{47}$$

$$b_{2,2} = \cos(\gamma_2)/[r_1 r_2 \sin(\gamma_1)\sin(\gamma_2)], \tag{48}$$

$$b_{2,3} = \cos(\gamma_1)/[r_1 r_2 \sin^2(\gamma_1)], \tag{49}$$

$$b_{3,1} = [r_3\cos(\gamma_2) - r_2\cos(\gamma_1)]/[2r_1^2 r_2\sin(\gamma_1)], \tag{50}$$

$$b_{3,2} = 1/[2r_1 r_2\sin(\gamma_1)], \tag{51}$$

$$b_{3,3} = -1/[2r_1 r_2\sin(\gamma_1)]. \tag{52}$$

The remaining coefficients for $i = 4,5,6$ can be estimated using the periodicity property.

References

[1] V.V. Aristov, Direct Methods for Solving the Boltzmann Equation and Study of Nonequilibrium Flows, Kluwer Academic Publishers., Dordrecht, The Netherlands, 2001.
[2] F. Tcheremissine, Direct numerical solution of the Boltzmann equation, RGD24 AIP Conference Proceedings 762 (2005) 677–685.
[3] F. Sharipov, G. Bertoldo, Numerical solution of the linearized Boltzmann equation for an arbitrary intermolecular potential, J. Comput. Phys. 228 (2009) 3345–3357.
[4] L. Mieussens, Discrete velocity models and numerical schemes for the Boltzmann–BGK equation in plane and axisymmetric geometries, J. Comput. Phys. 162 (2000) 429–466.
[5] P. Kowalczyk, A. Palczewski, G. Russo, Z. Walenta, Numerical solutions of the Boltzmann equation: comparison of different algorithms, Eur. J. Mech. B. Fluids 27 (2008) 62–74.
[6] S. Takata, S. Yasuda, S. Kosuge, K. Aoki, Numerical analysis of thermal-slip and diffusion-slip flows of a binary mixture of hard-sphere molecular gases, Phys. Fluids 12 (2003) 3745–3766.
[7] S. Naris, D. Valougeorgis, Boundary driven non-equilibrium gas flow in a grooved channel via kinetic theory, Phys. Fluids 19 (2007) 067103.1–067103.15.
[8] C. Cercignani, Slow Rarefied Flows: Theory and applications to Micro-electro-mechanical systems, Birkhauser Verlag, Basel, 2006.
[9] D. Valougeorgis, S. Naris, Acceleration schemes of the discrete velocity method: gaseous flows in rectangular microchannels, SIAM J. Sci. Comp. 25 (2003) 534–552.
[10] S. Naris, D. Valougeorgis, F. Sharipov, D. Kalempa, Discrete velocity modelling of gaseous mixture flows in MEMS, Superlattices and Microstructures 35 (2004) 629–643.
[11] J. Lihnaropoulos, S. Naris, D. Valougeorgis, Formulation and stability analysis of rapidly convergent iteration schemes for the 2-dimentional linearized BGK equation, Transp. Theory Stat. Phys. 36 (2007) 513–528.
[12] M.L. Adams, E.W. Larsen, Fast iterative methods for discrete-ordinates particle transport calculations, Prog. Nucl. Energy 40 (1) (2002) 3–159.

[13] D. Valougeorgis, M. Williams, E.W. Larsen, Stability analysis of synthetic acceleration methods with anisotropic scattering, Nucl. Sci. Eng. 99 (2) (1988) 91–98.
[14] S. Naris, D. Valougeorgis, Rarefied gas flow in a triangular duct based on a boundary fitted lattice, Eur. J. Mech. B. Fluids 27 (2008) 810–822.
[15] F. Sharipov, V. Seleznev, Data on internal rarefied gas flows, J. Phys. Chem. Ref. Data 27 (3) (1998) 657–706.
[16] F.J. McCormack, Construction of linearized kinetic models for gaseous mixtures and molecular gases, Phys. Fluids 16 (12) (1973) 2095–2105.
[17] S. Naris, D. Valougeorgis, F. Sharipov, D. Kalempa, Flow of gaseous mixtures through rectangular microchannels driven by pressure, temperature and concentration gradients, Phys. Fluids 17 (10) (2005) 100607.1–100607.12.
[18] F. Sharipov, Rarefied gas flow through a long rectangular channel, J. Vac. Sci. Technol., A 17 (5) (1999) 3062–3066.